Available online at www.sciencedirect.com
ScienceDirect
Journal of Sound and Vibration 305 (2007) 621–640
JOURNAL OF SOUND AND VIBRATION
www.elsevier.com/locate/jsvi

# Vibration analysis of the maglev guideway with the moving load

H.P. Wang*, J. Li, K. Zhang

*Maglev Engineering Center, National University of Defense Technology, Changsha Hunan 410073, China*

Received 17 December 2006; received in revised form 3 March 2007; accepted 15 April 2007
Available online 8 June 2007

**Abstract**

The response of the guideway induced by moving maglev vehicle is investigated in this paper. The maglev vehicle is simplified as evenly distributed force acting on the guideway at constant speed. According to the experimental line, the guideway structure of rail–sleeper–bridge is simplified as Bernoulli–Euler (B–E) beam—evenly distributed spring—simply supported B–E beam structure; thus, double deck model of the maglev guideway is constructed which can more accurately reflect the dynamic characteristic of the experimental line. The natural frequency and mode are deduced based on the theoretical model. The relationship between structural parameters and natural frequency are exploited by employing the numerical calculation method. The way to suppress the vehicle–guideway interaction by regulating the structural parameter is also discussed here. Using the normal coordinate transformation method, the coupled differential equations of motion of the maglev guideway are converted into a set of uncoupled equations. The closed-form solutions for the response of the guideway subjecting the moving load are derived. It is noted that the moving load would not induce the vehicle–guideway interaction oscillation. The analysis of the guideway impact factor implies that at some position of the guideway, the deflection may decrease with the increase of the speed of the load; several extreme value of the guideway displacement will appear induced by different speeds, with different acting place, the speeds are different either. The final numerical simulation verifies these conclusions.


## 1. Introduction

Maglev vehicle is one of the important transportation equipment of the urban track traffic system toward the future because of its safety and environmental friendly. But vehicle–guideway interaction problem bothers the investigators and engineers of the maglev system for years. No well-accepted interpretation has been reported yet. The solution of it is significant for reducing system cost and improving the running quality and can greatly accelerate the commercialization process of the maglev traffic system. The investigation of the guideway is the basement of this problem. Now most study simplifies the guideway to simply supported B–E beam, for example, Cai et al. [1–3], Zhao et al. [4] and Zheng et al. [5,6]. This railroad model can only solve one-dimension vibration of the elastic beam. It cannot accurately reflect the dynamic characteristic of the guideway system, which has much limitation in researching the vehicle–guideway interaction problem. Few results about the maglev track model considering the structure of rail–sleeper–bridge have been reported in present literature. It is our main concern in this article.

*Corresponding author. Fax: +86 0731 4516000.
*E-mail address:* nudtwhp@yahoo.com.cn (H.P. Wang).

0022-460X/$ - see front matter 
doi:10.1016/j.jsv.2007.04.030

Different from maglev traffic system, fruitful results have been achieved about the vehicle–bridge interaction with the fast development of the high-speed railway system. Yang et al. [7,8] simplifies the bridge as simply supported beam and studies the vehicle–bridge interaction problem based on the model of it. If the elasticity of the support is considered, resonances of much higher peaks can be excited by moving trains at much lower speeds than those on simply supported beams. In general, it is confirmed that accurate solutions can be obtained by considering only the first mode, which can greatly simplify the analysis process. Yau et al.'s research about vertical acceleration of simply supported beam shows that if the train runs at the resonant speed, the maximum impact acceleration may appear at the second or higher mode of the beam [9,10]. To find the influence of sleepers and ballast to the moving train, Baeza et al. [11] builds the railway model considering the contact of wheel–track, sleeper and ballast. Modal substructure approach is employed to study wheel–track interaction phenomenon. Biondi et al. [12] simplifies the sleeper and ballast as parallel spring-damping structure. Numerical method is applied to analyze the dynamics of train–track–bridge system. Shamalta et al. [13] analytically study the dynamic response of an embedded railway track to a moving load. Two-dimensional railway model is constructed and he uses Fourier integral transform to obtain the closed-form solution of the system. The book by Yang et al. [14] offers a comprehensive study on the mechanisms of resonance for train-induced vibrations on high-speed railway bridge [9].

Modeling the method of investigating the vehicle–track resonant problem of the wheel–track system, this paper makes middle-low speed maglev test line as researching object. The response of the maglev guideway induced by moving maglev vehicle is its main consideration. The deformation conditions of the guideway system are also investigated here. The sleeper is simplified as evenly distributed spring, two rails are merged into one free ends B–E beam, and the bridge is treated as simply supported B–E beam. Then the double deck model with the component of free-end beam, evenly distributed spring and simply supported beam is deduced, which can more accurately reflect the experimental guideway. Different from the point contact of the wheel–track system, the force of the maglev vehicle acting on the rail is distributed. In this article, the maglev vehicle is simplified as evenly distributed force with constant speed. Mode analyzing method is introduced to convert the continuous system equations into a set of multiple degrees of freedom coupling differential equations. Then mode superposition method is employed to decouple the coupling equations so that one order approximate closed-form solution of the guideway can be obtained. Finally, we use Wilson-$\theta$ numerical integral method to verify the analyzing results.

## 2. Constructing the model of the guideway

This section builds the theoretical model of the maglev guideway. According to the simplified condition proposed previously, sketch map of the maglev guideway is given in Fig. 1. Bridge and rail are connected by evenly distributed spring, the stiffness of per unit length is $k_{sle}$. $z_r$ and $z_b$ are, respectively, rail and bridge vertical displacement. The length of the bridge and rail is $L_b$. The bridge is simply support while the rail is free. The evenly distributed force represents the maglev vehicle moving at speed $v$, whose density of per unit length is $f_m$ and the length is $L_v$.

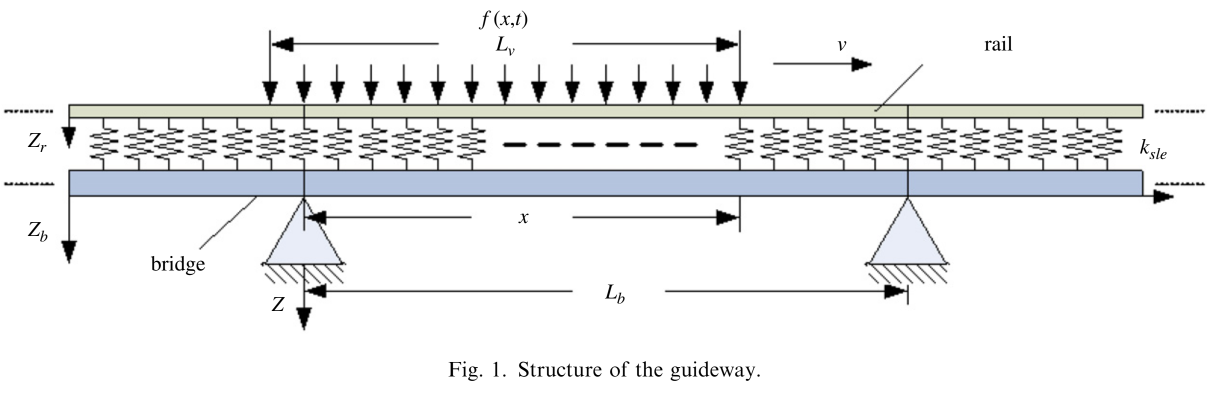


Fig. 1. Structure of the guideway.

Based on the above assumptions, the motion equations to describe deformation of the bridge and rail are

$$E_b I_b \frac{\partial^4 z_b(x,t)}{\partial x^4} + cb\frac{\partial z_b(x,t)}{\partial t} + \rho_b \frac{\partial^2 z_b(x,t)}{\partial t^2} = k_{sle}(z_r(x,t) - z_b(x,t)), \tag{1}$$

$$E_r I_r \frac{\partial^4 z_r(x,t)}{\partial x^4} + cr\frac{\partial z_r(x,t)}{\partial t} + \rho_r \frac{\partial^2 z_r(x,t)}{\partial t^2} = f(x,t) - k_{sle}(z_r(x,t) - z_b(x,t)), \tag{2}$$

where $E_b$ and $E_r$ are elastic modulus, $I_b$ and $I_r$ are moment of inertia, $cb$ and $cr$ are damping coefficient, $\rho_b$ and $\rho_r$ are the mass per unit length of the bridge and rail. According to the position on the rail, moving load $f(x,t)$ is written to be [16]

$$f(x,t) = f_m \begin{cases} 1 - H(x - vt) & \text{(running on to the bridge)}, \\ H(x - vt + L_v) - H(x - vt) & \text{(running on the bridge)}, \\ H(x - vt + L_v) & \text{(running out of the bridge)}, \end{cases} \tag{3}$$

where $H(t)$ is the unit step function, it describes a unit evenly distributed load. The effective length and position of it is determined by running speed $v$ and time $t$.

To get analytical solutions of the above partial differential equations, we need to simplify the high-order partial differential equations into a set of ordinary differential equation. After that, normal coordinate can be applied to estimate the vertical displacement of the rail and bridge.

## 3. Vibration analysis

To simplify the high-order partial differential equations, we use mode analyzing method. The displacement of the bridge $z_b(x,t)$ can be approximately expressed as

$$z_b(x,t) = \sum_{n=1} \phi_{b,n}(x) q_{b,n}(t), \tag{4}$$

where $\phi_{b,n}(x)$ is the $n$th shape of the bridge at position $x$, $q_{b,n}(t)$ denotes the generalized coordinates associated with the $n$th shape $\phi_{b,n}(x)$. Because the bridge is simply supported, the boundary conditions of it are

$$E_b I_b \phi''_{b,n}(0,t) = E_b I_b \phi''_{b,n}(L_b,t) = 0, \quad \phi_{b,n}(0,t) = \phi_{b,n}(L_b,t) = 0, \quad z_b(x,0) = \dot{z}_b(x,0) = 0. \tag{5}$$

According to this boundary condition (4) can be rewritten as

$$z_b(x,t) = \sum_{n=1} \phi_{b,n}(x) q_{b,n}(t) = \sum_{n=1} \sin\left(\frac{n\pi x}{L_b}\right) q_{b,n}(t). \tag{6}$$

Similarly, the displacement of the rail is determined by

$$z_r(x,t) = \sum_{n=1} \phi_{r,n}(x) q_{r,n}(t), \tag{7}$$

where $\phi_{r,n}(x)$ is the $n$th shape of the bridge at position $x$, $q_{r,n}(t)$ denotes the generalized coordinates associated with the $n$th shape $\phi_{r,n}(x)$. Because the two ends of the rail are free, the boundary conditions of it are

$$\phi''_{r,n}(0) = \phi''_{r,n}(L_b) = 0, \quad \phi'''_{r,n}(0) = \phi'''_{r,n}(L_b) = 0, \quad z_r(x,0) = \dot{z}_r(x,0) = 0. \tag{8}$$

According to Refs. [17,18], the specific shape of the rail is

$$\phi_{r,n}(x) = \cosh \lambda_n x + \cos \lambda_n x - V_n(\sinh \lambda_n x + \sin \lambda_n x), \ n = 1,2,3,\ldots . \tag{9}$$

where

$$V_n = \frac{\sinh \lambda_n L_b + \sin \lambda_n L_b}{\cosh \lambda_n L_b + \cos \lambda_n L_b}, \quad \lambda_n L_b \cong \left(n + \frac{1}{2}\right)\pi.$$

By substituting the displacement functions (6) and (9) into (1) and (2), then multiplying both sides of the equations with respect to the variation of the assumed shape functions, integrating the equations over the beam length $L_b$, and finally considering the mode orthogonal condition, we can derive the following simultaneous differential equations of motion in terms of the generalized coordinates ($q_{b,n}$, $q_{r,n}$) as

$$B_0\ddot{q}_{b,n} + B_1\dot{q}_{b,n} + B_{2,n}q_{b,n} - B_{3,n}q_{r,n} = \sum_{k=1,k\neq n} B_{4,k}q_{r,k}, \tag{10}$$

$$C_{0,n}\ddot{q}_{r,n} + C_{1,n}\dot{q}_{r,n} + C_{2,n}q_{r,n} - B_{3,n}q_{b,n} = \sum_{k=1,k\neq n} C_{4,k}q_{b,k} + C_{5,n}, \tag{11}$$

where

$$B_0 = \frac{\rho_b L_b}{2}, \quad C_{0,n} = \rho_r \bar{D}_n, \quad B_1 = \frac{crL_b}{2}, \quad C_{1,n} = cr\bar{D}_n, \quad B_{2,n} = \frac{E_b I_b n^4\pi^4 + k_{sle}L_b^4}{2L_b^3},$$

$$B_{3,n} = -2k_{sle}L_b n\frac{2+2V_n}{\pi(4n+1)} + 4k_{sle}L_b n\frac{1-\cosh(\pi(n+0.5))\cos(n\pi) + V_n\sinh(\pi(n+0.5))\cos(n\pi)}{\pi(8n^2+4n+1)},$$

$$B_{4,k} = 4k_{sle}L_b n\left(\frac{1+V_k\cos(n\pi)\cos(k\pi)}{\pi\left(4n^2-4k^2-4k-1\right)} + \frac{1-\cosh(k\pi+0.5\pi)\cos(n\pi) + V_k\sinh(k\pi+0.5\pi)\cos(n\pi)}{\pi\left(4n^2+4k^2+4k+1\right)}\right),$$

$$C_{2,n} = \left(\frac{E_r I_r \pi^4}{16L_b^4}(2n+1)^4 + k_{sle}\right)\bar{D}_n,$$

$$C_{4,k} = 4k_{sle}L_b k\left(\frac{1+V_n\cos(k\pi)\cos(n\pi)}{\pi\left(4k^2-4n^2-4n-1\right)} + \frac{1-\cosh(n\pi+0.5\pi)\cos(k\pi) + V_n\sinh(n\pi+0.5\pi)\cos(k\pi)}{\pi\left(4k^2+4n^2+4n+1\right)}\right),$$

$$\bar{D}_n = \frac{2L_b}{(2n+1)\pi}\left(\cos(n\pi)\cosh\left(\frac{2n+1}{2}\pi\right) + V_n^2\cos(n\pi)\cosh\left(\frac{2n+1}{2}\pi\right) - 4V_n\cos(n\pi)\sinh\left(\frac{2n+1}{2}\pi\right)\right)$$
$$+ \frac{-V_n L_b}{(2n+1)\pi} + L_b + \frac{L_b}{(2n+1)\pi}\left(\sinh(2n+1)\pi - 2V_n\cosh(2n+1)\pi + V_n^2\sinh(2n+1)\pi\right).$$

Considering different acting position of the load on the bridge, $C_{5,n}$ can be expressed as [16]:

(1) The load is running on to the bridge:

$$C_{5u,n} = \int_0^{vt} f(x,t)\phi_{r,n}(x)\,\mathrm{d}x = \frac{f_m}{\lambda_n}(\sinh(v\lambda_n t) + \sin(v\lambda_n t) - V_n(\cosh(v\lambda_n t) - \cos(v\lambda_n t))). \tag{12a}$$

(2) The load is running on the bridge:

$$\begin{aligned} C_{5a,n} &= \int_{vt-L_v}^{vt} f(x,t)\phi_{r,n}(x)\,\mathrm{d}x \\ &= \frac{f_m}{\lambda_n}(\sinh(v\lambda_n t) + \sin(v\lambda_n t) - V_n\cosh(v\lambda_n t) + V_n\cos(v\lambda_n t) - \sinh((vt-L_v)\lambda_n) \\ &\quad - \sin((vt-L_v)\lambda_n) + V_n\cosh((vt-L_v)\lambda_n) + V_n\cos((vt-L_v)\lambda_n)). \end{aligned} \tag{12b}$$

(3) The load is running out of the bridge:

$$\begin{aligned} C_{5o,n} &= \int_{vt-L_v}^{L_b} f(x,t)\phi_{r,n}(x)\,\mathrm{d}x \\ &= \frac{f_m}{\lambda_n}(-\sinh((vt-L_v)\lambda_n) - \sin((vt-L_v)\lambda_n) + V_n\cosh((vt-L_v)\lambda_n) - V_n\cos((vt-L_v)\lambda_n) + \\ &\quad \sinh(\lambda_n L_b) + \sin(\lambda_n L_b) - V_n\cosh(\lambda_n L_b) + V_n\cos(\lambda_n L_b)), \end{aligned} \tag{12c}$$

where

$$\lambda_n = \frac{(2n+1)\pi}{2L_b}.$$

Writing (10) and (11) into matrix form, we have the generalized coordinate equation of the guideway system about the time

$$\begin{bmatrix} B_0 & 0 \\ 0 & C_{0,n} \end{bmatrix}\begin{bmatrix} \ddot{q}_{b,n} \\ \ddot{q}_{r,n} \end{bmatrix} + \begin{bmatrix} B_1 & 0 \\ 0 & C_{1,n} \end{bmatrix}\begin{bmatrix} \dot{q}_{b,n} \\ \dot{q}_{r,n} \end{bmatrix} + \begin{bmatrix} B_{2,n} & -B_{3,n} \\ -B_{3,n} & C_{2,n} \end{bmatrix}\begin{bmatrix} q_{b,n} \\ q_{r,n} \end{bmatrix}$$
$$= \begin{bmatrix} \sum_{k=1,k\neq n} B_{4,k} q_{r,k} \\ \sum_{k=1,k\neq n} C_{4,k} q_{b,k} \end{bmatrix} + \begin{bmatrix} 0 \\ C_{5,n} \end{bmatrix}. \quad (13)$$

## 3.1. Free vibration analysis of the maglev guideway

To capture the dynamic characteristics of a vibrating system, free vibration analysis is one convenient way. By letting $B_{4,k} = C_{4,k} = 0$, $c_b = c_r = 0, f = 0$ in Eq. (13), the generalized equations for the maglev guideway is reduced to the following for free vibration:

$$\begin{bmatrix} B_0 & 0 \\ 0 & C_{0,n} \end{bmatrix}\begin{bmatrix} \ddot{q}_{b,n} \\ \ddot{q}_{r,n} \end{bmatrix} + \begin{bmatrix} B_{2,n} & -B_{3,n} \\ -B_{3,n} & C_{2,n} \end{bmatrix}\begin{bmatrix} q_{b,n} \\ q_{r,n} \end{bmatrix} = \begin{bmatrix} 0 \\ 0 \end{bmatrix}. \quad (14)$$

Consider only the first $n$ coupled equations in Eq. (14). By assuming the vibration to be of the harmonic type, the solution of (14) can be shown as

$$\begin{bmatrix} q_{b,n}(t) \\ q_{r,n}(t) \end{bmatrix} = \begin{bmatrix} \varphi_{b,n} \\ \varphi_{r,n} \end{bmatrix} \sin(\Omega_n t + \theta_n), \quad (15)$$

where $\varphi_{b,n}$ and $\varphi_{r,n}$ are vibration amplitude of the bridge and rail, $\Omega_n$ is the natural frequency, $\theta_n$ is the vibration phase. Referring to the initial condition given in Eqs. (5) and (8), it is easy to note that $\theta_n = 0$. If (15) stands, next condition must be satisfied:

$$\begin{bmatrix} B_{2,n} - B_0\Omega^2 & -B_{3,n} \\ -B_{3,n} & C_{2,n} - C_{0,n}\Omega^2 \end{bmatrix}\begin{bmatrix} \varphi_{b,n} \\ \varphi_{r,n} \end{bmatrix} = \mathbf{0}. \quad (16)$$

If (16) has non-zero solution, then

$$\begin{vmatrix} B_{2,n} - B_0\Omega^2 & -B_{3,n} \\ -B_{3,n} & C_{2,n} - C_{0,n}\Omega^2 \end{vmatrix} = 0. \quad (17)$$

Expanding it yields

$$\left(\Omega_n^2\right)^2 B_0 C_{0,n} - \Omega_n^2\left(B_0 C_{2,n} + B_{2,n} C_{0,n}\right) - B_{3,n}^2 + B_{2,n} C_{2,n} = 0. \quad (18)$$

Eq. (18) is quadratic equation about $\Omega_n^2$, from it, a couple of root can be obtained as

$$\Omega_{n,1,2}^2 = \frac{1}{2B_0 C_{0,n}}\left(\bar{B}_n \pm \bar{C}_n\right), \quad (19)$$

where $\bar{B}_n = B_{2,n}C_{0,n} + B_0 C_{2,n}$, $\bar{C}_n = \sqrt{B_{2,n}^2 C_{0,n}^2 - 2B_{2,n}C_{0,n}B_0 C_{2,n} + B_0^2 C_{2,n}^2 + 4B_0 C_{0,n} B_{3,n}^2}$. If $n$ equals to a known integer, according to the expression of (19), (18) has a pair of positive roots, which means that the guideway system may exhibit two types of synchronization free oscillation with different frequency $\Omega_{n,1}$ or $\Omega_{n,2}$. We name the smaller one the first natural frequency and the bigger one the second natural frequency of the $n$th mode. Corresponding vibration are called the first natural vibration and the second natural vibration.

Substituting $\Omega^2_{n,1}$ and $\Omega^2_{n,2}$ into (16), two real vectors $\boldsymbol{\varphi}_{n1}$and $\boldsymbol{\varphi}_{n2}$ can be determined as

$$\boldsymbol{\varphi}_{n1} = \begin{bmatrix} \varphi_{b,n11} \\ \varphi_{r,n11} \end{bmatrix}, \quad \boldsymbol{\varphi}_{n2} = \begin{bmatrix} \varphi_{b,n12} \\ \varphi_{r,n12} \end{bmatrix}, \tag{20}$$

$\varphi_{b,n11}$ and $\varphi_{r,n11}$, elements of $\boldsymbol{\varphi}_{n1}$, satisfy

$$\begin{cases} \left(B_{2,n} - \dfrac{1}{2C_{0,n}}(\bar{B}_n - \bar{C}_n)\right)\varphi_{b,n11} - B_{3,n}\varphi_{r,n11} = 0, \\ -B_{3,n}\varphi_{b,n11} + \left(C_{2,n} - \dfrac{1}{2B_0}(\bar{B}_n - \bar{C}_n)\right)\varphi_{r,n11} = 0. \end{cases} \tag{21}$$

Because $\Omega^2_{n,1}$ is the root of (16) where the determinant of its coefficient matrix equals to zero, (16) has infinite number of non-zero roots. So $\varphi_{b,n11}$ and $\varphi_{r,n11}$ cannot be specifically determined. Only the amplitude proportion of the first natural vibration of the guideway system can be obtained:

$$\psi_{n1} = \frac{\varphi_{r,n11}}{\varphi_{b,n11}} = \frac{2B_{2,n}C_{0,n} - \left(\bar{B}_n - \bar{C}_n\right)}{2B_{3,n}C_{0,n}} = \frac{2B_0B_{3,n}}{2B_0C_{2,n} - \left(\bar{B}_n - \bar{C}_n\right)}. \tag{22}$$

Following the same procedure, amplitude proportion of the second natural vibration is

$$\psi_{n2} = \frac{\varphi_{r,n12}}{\varphi_{b,n12}} = \frac{2B_{2,n}C_{0,n} - \left(\bar{B}_n + \bar{C}_n\right)}{2B_{3,n}C_{0,n}} = \frac{2B_0B_{3,n}}{2B_0C_{2,n} - \left(\bar{B}_n + \bar{C}_n\right)}. \tag{23}$$

Vectors

$$\boldsymbol{\varphi}_{n1} = \varphi_{b,n11}\begin{bmatrix} 1 \\ \psi_{n1} \end{bmatrix} \quad \text{and} \quad \boldsymbol{\varphi}_{n2} = \varphi_{b,n12}\begin{bmatrix} 1 \\ \psi_{n2} \end{bmatrix}$$

reflect the character of the guideway system when it vibrates at natural frequency and so is called vibration mode of the first and second natural vibration.

Natural vibration mode $\boldsymbol{\varphi}_{nr}$ $r = 1{,}2$ gives the proportion relation of the rail and bridge. When the guideway vibrates at the $r$th natural frequency, it means that the natural vibration is always the intermittent vibration with the same frequency, but the vibration may be in-phase ($\psi_{nr}<0$) or anti-phase ($\psi_{nr}<0$). For any 7natural vibration mode $\varphi_{nr}$ and non-zero real constant $a$, $a\boldsymbol{\varphi}_{nr}$ is still the natural vibration mode corresponding to $\Omega_{n,r}$ [17].

To decouple the coupling equations, normal coordinate transformation is employed so that generalized coordinate $[q_b\ q_r]^{\mathrm{T}}$ can be expressed by normal coordinate $\mathbf{Q} = [Q_b\ Q_r]^{\mathrm{T}}$as

$$\mathbf{q} = \begin{bmatrix} q_{b,n} \\ q_{r,n} \end{bmatrix} = \begin{bmatrix} 1 & 1 \\ \psi_{n1} & \psi_{n2} \end{bmatrix}\begin{bmatrix} Q_{b,n} \\ Q_{r,n} \end{bmatrix} = \boldsymbol{\Psi}_n\mathbf{Q}, \tag{24}$$

where $\boldsymbol{\Psi}_n$ is the transformation matrix from $\mathbf{q}$ to $\mathbf{Q}$.

Notes: the above analysis assumes that there is no coupling among different vibration mode of the guideway, only the coupling between the same vibration mode is discussed. If letting $c_b = c_r = 0$, $f = 0$, (13) becomes

$$\begin{bmatrix} B_0 & 0 \\ 0 & C_{0,n} \end{bmatrix}\begin{bmatrix} \ddot{q}_{b,n} \\ \ddot{q}_{r,n} \end{bmatrix} + \begin{bmatrix} B_{2,n} & -B_{3,n} \\ -B_{3,n} & C_{2,n} \end{bmatrix}\begin{bmatrix} q_{b,n} \\ q_{r,n} \end{bmatrix} = \begin{bmatrix} \sum_{k=1,k\neq n} B_{4,k}q_{r,k} \\ \sum_{k=1,k\neq n} C_{4,k}q_{r,k} \end{bmatrix}. \tag{25}$$

If $n\geqslant 2$, coupling exist among different modes. And low modes influence the high modes. Assuming mode method can be used to get the first mode closed-form solutions. Then higher mode closed-form solutions can always be obtained by solving the lower ones. It includes the low order exciting part. To get the pure high-order mode closed-form solutions, we set $B_{4,k} = C_{4,k} = 0$.

### 3.2. Midpoint displacement response of the maglev guideway

In general, for a simply supported beam subjected to moving load, the maximum deflection response will be excited at the mid-span [10,15]. Therefore, the first set of displacement shapes can be used to compute the midpoint deflection response of the guideway under the moving load. In other words, (13) is reduced to

$$\begin{bmatrix} B_0 & 0 \\ 0 & C_{0,1} \end{bmatrix}\begin{bmatrix} \ddot{q}_{b,1} \\ \ddot{q}_{r,1} \end{bmatrix} + \begin{bmatrix} B_1 & 0 \\ 0 & C_{1,1} \end{bmatrix}\begin{bmatrix} \dot{q}_{b,1} \\ \dot{q}_{r,1} \end{bmatrix} + \begin{bmatrix} B_{2,1} & -B_{3,1} \\ -B_{3,1} & C_{2,1} \end{bmatrix}\begin{bmatrix} q_{b,1} \\ q_{r,1} \end{bmatrix} = \begin{bmatrix} 0 \\ C_{5,1} \end{bmatrix}. \tag{26}$$

Observing the coefficient of (26), we know that

$$\frac{B_1}{B_0} = \frac{c_b}{\rho_b}, \quad \frac{C_1}{C_0} = \frac{c_r}{\rho_r}. \tag{27}$$

Because the structure damping of the rail and bridge is small, we assume

$$a_0 = \frac{c_b}{\rho_b} \approx \frac{c_r}{\rho_r}. \tag{28}$$

Then the damping of (26) is called mass damping, substituting it into (26) yields

$$\begin{bmatrix} B_0 & 0 \\ 0 & C_{0,1} \end{bmatrix}\begin{bmatrix} \ddot{q}_{b,1} \\ \ddot{q}_{r,1} \end{bmatrix} + a_0\begin{bmatrix} B_0 & 0 \\ 0 & C_{0,1} \end{bmatrix}\begin{bmatrix} \dot{q}_{b,1} \\ \dot{q}_{r,1} \end{bmatrix} + \begin{bmatrix} B_{2,1} & -B_{3,1} \\ -B_{3,1} & C_{2,1} \end{bmatrix}\begin{bmatrix} q_{b,1} \\ q_{r,1} \end{bmatrix} = \begin{bmatrix} 0 \\ C_{5,1} \end{bmatrix}. \tag{29}$$

Eq. (29) shows that the rail and bridge couple each other because of the distributed spring, to deduce their closed-form solutions, normal coordinate transformation method is employed to convert the coupling equations into a set of uncoupling equations. Substituting (25) into (29) and multiplying both side with $\mathbf{\Psi}_1^{\mathrm{T}}$, if orthogonal condition of the natural modal is considered, (29) becomes

$$\begin{bmatrix} m_b & 0 \\ 0 & m_r \end{bmatrix}\begin{bmatrix} \ddot{Q}_b \\ \ddot{Q}_r \end{bmatrix} + \begin{bmatrix} c_b & 0 \\ 0 & c_r \end{bmatrix}\begin{bmatrix} \dot{Q}_b \\ \dot{Q}_r \end{bmatrix} + \begin{bmatrix} k_b & 0 \\ 0 & k_r \end{bmatrix}\begin{bmatrix} Q_b \\ Q_r \end{bmatrix} = \begin{bmatrix} \psi_{11} \\ \psi_{12} \end{bmatrix} C_{5,1}, \tag{30}$$

where $m_b = B_0 + \psi_{11}^2 C_{0,1}$, $m_r = B_0 + \psi_{12}^2 C_{0,1}$, $c_b = a_0(B_0 + \psi_{11}^2 C_{0,1})$, $c_r = a_0(B_0 + \psi_{12}^2 C_{0,1})$, $k_b = B_{2,1} - 2B_{3,1}\psi_{11} + C_{2,1}\psi_{11}^2$, $k_r = B_{2,1} - 2B_{3,1}\psi_{12} + C_{2,1}\psi_{12}^2$. Initial conditions of the generalized coordinate are known as

$$\begin{bmatrix} q_b \\ q_r \end{bmatrix} = \begin{bmatrix} 0 \\ 0 \end{bmatrix}, \quad \begin{bmatrix} \dot{q}_b \\ \dot{q}_r \end{bmatrix} = \begin{bmatrix} 0 \\ 0 \end{bmatrix}. \tag{31}$$

Substituting it into (25), the initial conditions of the normal coordinate is

$$\begin{bmatrix} Q_b \\ Q_r \end{bmatrix} = \begin{bmatrix} 0 \\ 0 \end{bmatrix}, \quad \begin{bmatrix} \dot{Q}_b \\ \dot{Q}_r \end{bmatrix} = \begin{bmatrix} 0 \\ 0 \end{bmatrix}. \tag{32}$$

As is shown in Eq. (12), when the position of the distributed moving load is different, the expression of $C_{5,1}$ is different either. Then the solutions of (30) must be respectively considered according to the position of the moving load. Laplace transformation is applied to get the solutions of (30):

(1) The load is running on to the bridge: Eq. (32) has shown the initial condition of (30), transform both side of (30) into Laplace domain yields

$$Q_{ub}(s)\left(m_b s^2 + c_b s + k_b\right) = \frac{f_m \psi_{11}}{\lambda_1}\left(\frac{\omega_1 - V_1 s}{s^2 - \omega_1^2} + \frac{V_1 s - \omega_1}{s^2 + \omega_1^2}\right), \tag{33a}$$

$$Q_{ur}(s)\left(m_r s^2 + c_r s + k_r\right) = \frac{f_m \psi_{12}}{\lambda_1}\left(\frac{\omega_1 - V_1 s}{s^2 - \omega_1^2} + \frac{V_1 s - \omega_1}{s^2 + \omega_1^2}\right), \tag{33b}$$

where $\omega_1 = v\lambda_1$, it is the excitation frequency of the moving load. Then $Q_{ub}(s)$ and $Q_{ur}(s)$ can be written as the sum of rational fraction

$$Q_{ub}(s) = \frac{f_m\psi_{11}}{\lambda_1}\left(\frac{(m_b p_{ub1}p_{ub4} + m_b p_{ub0}p_{ub5})s + p_{ub2}p_{ub4} + p_{ub0}p_{ub6}}{p_{ub0}p_{ub4}(m_b s^2 + c_b s + k_b)} - \frac{p_{ub1}s + p_{ub3}}{p_{ub0}(s^2 - \omega_1^2)} + \frac{-p_{ub5}s + p_{ub7}}{p_{ub4}(s^2 + \omega_1^2)}\right), \tag{34a}$$

$$Q_{ur}(s) = \frac{f_m\psi_{12}}{\lambda_1}\left(\frac{(m_r p_{ur1}p_{ur4} + m_r p_{ur5}p_{ur0})s + p_{ur2}p_{ur4} + p_{ur0}p_{ur6}}{p_{ur0}p_{ur4}(m_r s^2 + c_r s + k_r)} - \frac{p_{ur1}s + p_{ur3}}{p_{r0}(s^2 - \omega_1^2)} + \frac{-p_{ur5}s + p_{ur7}}{p_{ur4}(s^2 + \omega_1^2)}\right), \tag{34b}$$

where $p_{ub0}$–$p_{ub7}$ and $p_{ur0}$–$p_{ur7}$ are given in the appendix. Applying Laplace inverse transformation to (34) yields

$$\begin{aligned} Q_{ub}(t) = \frac{f_m\psi_{11}}{\lambda_1}\Bigg(&\exp\left(-\frac{c_b}{2m_b}t\right)\Bigg(\left(\frac{p_{ub1}}{p_{ub0}} + \frac{p_{ub5}}{p_{ub4}}\right)\cos\left(\frac{\sqrt{4k_b m_b - c_b^2}}{2m_b}t\right) \\ &+ \frac{2\left(\frac{p_{ub2}}{p_{ub0}} + \frac{p_{ub6}}{p_{ub4}}\right) - c_b\left(\frac{p_{ub1}}{p_{ub0}} + \frac{p_{ub5}}{p_{ub4}}\right)}{\sqrt{4k_b m_b - c_b^2}}\sin\left(\frac{\sqrt{4k_b m_b - c_b^2}}{2m_b}t\right)\Bigg) \\ &- \frac{\exp(\omega_1 t)}{2}\left(\frac{p_{ub1}}{p_{ub0}} + \frac{p_{ub3}}{p_{ub0}\omega_1}\right) + \frac{\exp(-\omega_1 t)}{2}\left(-\frac{p_{ub1}}{p_{ub0}} + \frac{p_{ub3}}{p_{ub0}\omega_1}\right) \\ &+ \frac{p_{ub7}}{p_{ub4}\omega_1}\sin(\omega_1 t) - \frac{p_{ub5}}{p_{ub4}}\cos(\omega_1 t)\Bigg), \end{aligned} \tag{35a}$$

$$\begin{aligned} Q_{ur}(t) = \frac{f_m\psi_{12}}{\lambda_1}\Bigg(&\exp\left(-\frac{c_r}{2m_r}t\right)\Bigg(\left(\frac{p_{ur1}}{p_{ur0}} + \frac{p_{ur5}}{p_{ur4}}\right)\cos\left(\frac{\sqrt{4k_r m_r - c_r^2}}{2m_r}t\right) \\ &+ \frac{2\left(\frac{p_{ur2}}{p_{ur0}} + \frac{p_{ur6}}{p_{ur4}}\right) - c_r\left(\frac{p_{ur1}}{p_{ur0}} + \frac{p_{ur5}}{p_{ur4}}\right)}{\sqrt{4k_r m_r - c_r^2}}\sin\left(\frac{\sqrt{4k_r m_r - c_r^2}}{2m_r}t\right)\Bigg) \\ &- \frac{\exp(\omega_1 t)}{2}\left(\frac{p_{ur1}}{p_{ur0}} + \frac{p_{ur3}}{p_{ur0}\omega_1}\right) + \frac{\exp(-\omega_1 t)}{2}\left(-\frac{p_{ur1}}{p_{ur0}} + \frac{p_{ur3}}{p_{ur0}\omega_1}\right) \\ &+ \frac{p_{ur7}}{p_{ur4}\omega_1}\sin(\omega_1 t) - \frac{p_{ur5}}{p_{ur4}}\cos(\omega_1 t)\Bigg), \end{aligned} \tag{35b}$$

(2) The load is running on the bridge: Expanding (12b) yields

$$C_{5a,1} = a_1 \sinh(\omega_1 t) + a_2 \sin(\omega_1 t) + a_3 \cosh(\omega_1 t) + a_4 \cos(\omega_1 t), \tag{36}$$

where $a_1$–$a_4$ are given in the appendix. With the same procedure, Laplace transformation of (30) gets

$$Q_{ab}(s)\left(m_b s^2 + c_b s + k_b\right) = \psi_{11}\left(\frac{a_3 s + a_1\omega_1}{s^2 - \omega_1^2} + \frac{a_4 s + a_2\omega_1}{s^2 + \omega_1^2}\right), \tag{37a}$$

$$Q_{ar}(s)\left(m_r s^2 + c_r s + k_r\right) = \psi_{12}\left(\frac{a_3 s + a_1\omega_1}{s^2 - \omega_1^2} + \frac{a_4 s + a_2\omega_1}{s^2 + \omega_1^2}\right). \tag{37b}$$

The sum of rational fraction of $Q_{ab}(s)$ and $Q_{ar}(s)$ are

$$\begin{aligned} Q_{ab}(s) = \psi_{11}\Bigg( & \frac{\left(m_b p_{ab1} p_{ab4} + m_b p_{ab5} p_{ab0}\right)s + p_{ab2} p_{ab4} + p_{ab6} p_{ab0}}{p_{ab0} p_{ab4}\left(m_b s^2 + c_b s + k_b\right)} \\ & + \frac{-p_{ab1} s + p_{ab3}}{p_{ab0}\left(s^2 - \omega_1^2\right)} + \frac{-p_{ab5} s + p_{ab7}}{p_{ab4}\left(s^2 - \omega_1^2\right)}\Bigg), \end{aligned} \tag{38a}$$

$$\begin{aligned} Q_{ar}(s) = \psi_{12}\Bigg( & \frac{\left(m_r p_{ar1} p_{ar4} + m_b p_{ar5} p_{ar0}\right)s + p_{ar2} p_{ar4} + p_{ar0} p_{ar6}}{p_{ar0} p_{ar4}\left(m_r s^2 + c_r s + k_r\right)} \\ & + \frac{-p_{ar1} s + p_{ar3}}{p_{ar0}\left(s^2 - \omega_1^2\right)} + \frac{-p_{ar5} s + p_{ar7}}{p_{ar4}\left(s^2 - \omega_1^2\right)}\Bigg), \end{aligned} \tag{38b}$$

where $p_{ab0}$–$p_{ab7}$ and $p_{ar0}$–$p_{ar7}$ are given in the appendix. Applying Laplace inverse transformation to (38) yields

$$\begin{aligned} Q_{ab}(t) = \psi_{11}\Bigg( & \exp\left(-\frac{c_b}{2m_b}t\right)\Bigg(\left(\frac{p_{ab1}}{p_{ab0}} + \frac{p_{ab5}}{p_{ab4}}\right)\cos\left(\frac{\sqrt{4k_b m_b - c_b^2}}{2m_b}t\right) \\ & + \frac{2\left(\frac{p_{ab2}}{p_{ab0}} + \frac{p_{ab6}}{p_{ab4}}\right) - c_b\left(\frac{p_{ab1}}{p_{ab0}} + \frac{p_{ab5}}{p_{ab4}}\right)}{\sqrt{4k_b m_b - c_b^2}}\sin\left(\frac{\sqrt{4k_b m_b - c_b^2}}{2m_b}t\right)\Bigg) \\ & - \frac{\exp(\omega_1 t)}{2}\left(\frac{p_{ab1}}{p_{ab0}} - \frac{p_{ab3}}{p_{ab0}\omega_1}\right) + \frac{\exp(-\omega_1 t)}{2}\left(-\frac{p_{ab1}}{p_{ab0}} - \frac{p_{ab3}}{p_{ab0}\omega_1}\right) \\ & + \frac{p_{ab7}}{p_{ab4}\omega_1}\sin(\omega_1 t) - \frac{p_{ab5}}{p_{ab4}}\cos(\omega_1 t)\Bigg), \end{aligned} \tag{39a}$$

$$\begin{aligned} Q_{ar}(t) = \psi_{12}\Bigg( & \exp\left(-\frac{c_r}{2m_r}t\right)\Bigg(\left(\frac{p_{ar1}}{p_{ar0}} + \frac{p_{ar5}}{p_{ar4}}\right)\cos\left(\frac{\sqrt{4k_r m_r - c_r^2}}{2m_r}t\right) \\ & + \frac{2\left(\frac{p_{ar2}}{p_{ar0}} + \frac{p_{ar6}}{p_{ar4}}\right) - c_r\left(\frac{p_{ar1}}{p_{ar0}} + \frac{p_{ar5}}{p_{ar4}}\right)}{\sqrt{4k_r m_r - c_r^2}}\sin\left(\frac{\sqrt{4k_r m_r - c_r^2}}{2m_r}t\right)\Bigg) \end{aligned}$$

$$-\frac{\exp(\omega_1 t)}{2}\left(\frac{p_{ar1}}{p_{ar0}}-\frac{p_{ar3}}{p_{ar0}\omega_1}\right)+\frac{\exp(-\omega_1 t)}{2}\left(-\frac{p_{ar1}}{p_{ar0}}-\frac{p_{ar3}}{p_{ar0}\omega_1}\right)$$
$$\left.+\frac{p_{ar7}}{p_{ar4}\omega_1}\sin(\omega_1 t)-\frac{p_{ar5}}{p_{ar4}}\cos(\omega_1 t)\right), \tag{39b}$$

(3) The load is running out of the bridge: Expanding (12c) yields

$$C_{5o,1}=o_1\sinh(\omega_1 t)+o_2\sin(\omega_1 t)+o_3\cosh(\omega_1 t)+o_4\cos(\omega_1 t)+o_0, \tag{40}$$

where $o_0$–$o_4$ are given in the appendix. Laplace transformation of (30) is

$$Q_{ob}(s)\left(m_b s^2+c_b s+k_b\right)=\psi_{11}\left(\frac{o_3 s+o_1\omega_1}{s^2-\omega_1^2}+\frac{o_4 s+o_2\omega_1}{s^2+\omega_1^2}+\frac{o_0}{s}\right), \tag{41a}$$

$$Q_{or}(s)\left(m_r s^2+c_r s+k_r\right)=\psi_{12}\left(\frac{o_3 s+o_1\omega_1}{s^2-\omega_1^2}+\frac{o_4 s+o_2\omega_1}{s^2+\omega_1^2}+\frac{o_0}{s}\right). \tag{41b}$$

The sum of rational fraction of $Q_{ob}(s)$ and $Q_{or}(s)$ are

$$Q_{ob}(s)=\psi_{11}\left(\frac{\left(m_b k_b p_{ob1}p_{ob4}+m_b k_b p_{ob5}p_{ob0}-o_0 m_b p_{ob0}p_{ob4}\right)s+k_b p_{ob2}p_{ob4}+k_b p_{ob6}p_{ob0}-o_0 c_b p_{ob0}p_{ob4}}{k_b p_{ob0}p_{ob4}(m_b s^2+c_b s+k_b)}\right.$$
$$\left.+\frac{-p_{ob1}s+p_{ob3}}{p_{ob0}\left(s^2-\omega_1^2\right)}+\frac{-p_{ob5}s+p_{ob7}}{p_{ob4}\left(s^2-\omega_1^2\right)}+\frac{o_0}{k_b s}\right), \tag{42a}$$

$$Q_{or}(s)=\psi_{12}\left(\frac{\left(m_r k_r p_{or1}p_{or4}+m_r k_r p_{or5}p_{or0}-o_0 m_r p_{or0}p_{or4}\right)s+k_r p_{or2}p_{or4}+k_r p_{or0}p_{or6}-o_0 c_r p_{or0}p_{or4}}{k_r p_{or0}p_{or4}(m_r s^2+c_r s+k_r)}\right.$$
$$\left.+\frac{-p_{or1}s+p_{or3}}{p_{or0}\left(s^2-\omega_1^2\right)}+\frac{-p_{or5}s+p_{or7}}{p_{or4}\left(s^2-\omega_1^2\right)}+\frac{o_0}{k_r s}\right), \tag{42b}$$

where $p_{ob0}$–$p_{ob7}$ and $p_{or0}$–$p_{or7}$ are given in the appendix. Applying Laplace inverse transformation to (42) yields

$$Q_{ob}(t)=\psi_{11}\left(\exp\left(-\frac{c_b}{2m_b}t\right)\left(\left(\frac{p_{ob1}}{p_{ob0}}+\frac{p_{ob5}}{p_{ob4}}-\frac{o_0 m_b}{k_b}\right)\cos\left(\frac{\sqrt{4k_b m_b-c_b^2}}{2m_b}t\right)\right.\right.$$
$$\left.+\frac{2\left(\frac{p_{ob2}}{p_{ob0}}+\frac{p_{ob6}}{p_{ob4}}-\frac{o_0 c_b}{k_b}\right)-c_b\left(\frac{p_{ob1}}{p_{ob0}}+\frac{p_{ob5}}{p_{ob4}}-\frac{o_0 m_b}{k_b}\right)}{\sqrt{4k_b m_b-c_b^2}}\sin\left(\frac{\sqrt{4k_b m_b-c_b^2}}{2m_b}t\right)\right)$$
$$-\frac{\exp(\omega_1 t)}{2}\left(\frac{p_{ob1}}{p_{ob0}}-\frac{p_{ob3}}{p_{ob0}\omega_1}\right)+\frac{\exp(-\omega_1 t)}{2}\left(-\frac{p_{ob1}}{p_{ob0}}-\frac{p_{ob3}}{p_{ob0}\omega_1}\right)$$
$$\left.+\frac{p_{ob7}}{p_{ob4}\omega_1}\sin(\omega_1 t)-\frac{p_{ob5}}{p_{ob4}}\cos(\omega_1 t)+\frac{o_0}{k_b}\right), \tag{43a}$$

$$
\begin{aligned}
Q_{or}(t) = \psi_{12}\Bigg( & \exp\left(-\frac{c_r}{2m_r}t\right)\Bigg(\left(\frac{p_{or1}}{p_{or0}}+\frac{p_{or5}}{p_{or4}}-\frac{o_0 m_r}{k_r}\right)\cos\left(\frac{\sqrt{4k_r m_r - c_r^2}}{2m_r}t\right) \\
& + \frac{2\left(\frac{p_{or2}}{p_{or0}}+\frac{p_{or6}}{p_{or4}}-\frac{o_0 c_r}{k_r}\right) - c_r\left(\frac{p_{or1}}{p_{or0}}+\frac{p_{or5}}{p_{or4}}-\frac{o_0 m_r}{k_r}\right)}{\sqrt{4k_r m_r - c_r^2}}\sin\left(\frac{\sqrt{4k_r m_r - c_r^2}}{2m_r}t\right)\Bigg) \\
& - \frac{\exp(\omega_1 t)}{2}\left(\frac{p_{or1}}{p_{or0}}-\frac{p_{or3}}{p_{or0}\omega_1}\right) + \frac{\exp(-\omega_1 t)}{2}\left(-\frac{p_{or1}}{p_{or0}}-\frac{p_{or3}}{p_{or0}\omega_1}\right) \\
& + \frac{p_{or7}}{p_{or4}\omega_1}\sin(\omega_1 t) - \frac{p_{or5}}{p_{or4}}\cos(\omega_1 t) + \frac{o_0}{k_r}\Bigg). \qquad (43b)
\end{aligned}
$$

After the complex solving procedure given above, the closed-form solutions of the normal coordinate have been deduced. The dynamic response of the system includes transient and static two parts. The transient part will disappear with the time going on. Only static part is left. So in the following analysis, we just discuss the static part.

Substituting (35), (39) and (43) into (25), the generalized coordinate can be expressed as

$$
\begin{bmatrix} q_b \\ q_r \end{bmatrix} = \begin{bmatrix} Q_b + Q_r \\ \psi_{11}Q_b + \psi_{12}Q_r \end{bmatrix}. \qquad (44)
$$

Therefore, the midpoint deflection responses of the rail and bridge can, respectively, be approximated as

$$
z_b\left(\frac{L_b}{2}, t\right) \cong q_b, \qquad (45a)
$$

$$
z_r\left(\frac{L_b}{2}, t\right) \cong -1.2119\, q_r. \qquad (45b)
$$

It is easy to know that the speed of the moving load $v > 0$. Observing (35), (39) and (43), if any one of $p_{b0}$, $p_{r0}$, $p_{b4}$ and $p_{r4}$ equals to zero, $q_b, q_r \to \infty$ when $v$ equals to certain value. Previous section assumes the damping of the rail and bridge to be small. From their expression we know that $p_{b0}$, $p_{r0}$, $p_{b4}$ and $p_{r4}$ are always positive, which means $q_b, q_r \to \infty$ will not occur. It is noted that exponential term $e^{v\lambda_1 t}$ is included in the closed-form solutions and $\max(vt) = L_b$, which indicates that with the time going on, the vibration amplitude of the guideway will not increase infinitely.

Comprehensively analyzing the closed-form solutions indicates that when the evenly distributed load passes through the bridge, displacement of the guideway will arise. The displacement is composed of exponential and harmonic terms. Because the time length the load passing through the bridge is finite, the displacement of the guideway will not infinitely increase. All these indicate that vehicle–guideway interaction may not appear as is shown in Refs. [10,15] when the evenly distributed load passes through the bridge. In another way, excitation frequency $\omega_1$ of the moving load is determined by running speed and vibration modal. The bridge does not affect it. It increases with the increase of the speed and decrease with the increase of the rail length.

### 3.3. Displacement of high bending mode

The above analysis has obtained the first mode approximate solution. When $n = 2$, making the approximate solution as the known excitation, using $\boldsymbol{\psi}_2$ to decouple the coupling differential equations, following the same procedure, the second mode approximate solution can be solved. Similarly, any mode approximate solution is able to be solved theoretically. But high-order modes are always excited by low-order modes, this makes the analytical solution to be complicated and it is a hard work to analyze the results. So in this paper, only the first mode approximate solution is studied, high-order modes are investigated by numerical method.

## 4. Impact factor and speed parameter

The impact factor [7,8,15], defined as the ratio of the maximum dynamic to the maximum static response of the bridge under the same load minus one, are used to evaluate the dynamic response of the bridge due to the moving vehicular loads. One typical definition for the impact factor is

$$I = \frac{R_d(x) - R_s(x)}{R_s(x)}, \tag{46}$$

where $R_d(x)$ and $R_s(x)$, respectively, denote the maximum dynamic and static responses of the bridge calculated at the cross-section $x$ of the bridge of the interest. The speed parameter $S$ is also a useful parameter in analyzing the vehicle-induced vibrations, which is defined as the ration of the excitation frequency of the moving vehicle $\omega_1$ to the fundamental frequency $\Omega_{1,1}$ of the guideway, i.e.

$$S = \pi v/(L_b \Omega_{1,1}). \tag{47}$$

It is known that when the midpoint of the static evenly distributed load overlaps with the midpoint of the guideway, the static displacement of the guideway is maximal. Recalling the above analysis, the normal coordinates of the guideway to reflect the maximum static deflection are known as

$$\begin{aligned} Q_{b\text{mid}} = \frac{2f_m \psi_{11}}{\lambda_1 k_b} \bigg( & \cosh\left(\frac{1}{2}\lambda_1 L_b\right) \sinh\left(\frac{1}{2}\lambda_1 L_v\right) + \cos\left(\frac{1}{2}\lambda_1 L_b\right) \sin\left(\frac{1}{2}\lambda_1 L_v\right) \\ & - V_1 \left( \sinh\left(\frac{1}{2}\lambda_1 L_b\right) \sinh\left(\frac{1}{2}\lambda_1 L_v\right) + \sin\left(\frac{1}{2}\lambda_1 L_b\right) \sin\left(\frac{1}{2}\lambda_1 L_v\right)\right)\bigg), \end{aligned} \tag{48a}$$

$$\begin{aligned} Q_{r\text{mid}} = \frac{2f_m \psi_{12}}{\lambda_1 k_r} \bigg( & \cosh\left(\frac{1}{2}\lambda_1 L_b\right) \sinh\left(\frac{1}{2}\lambda_1 L_v\right) + \cos\left(\frac{1}{2}\lambda_1 L_b\right) \sin\left(\frac{1}{2}\lambda_1 L_v\right) \\ & - V_1 \left( \sinh\left(\frac{1}{2}\lambda_1 L_b\right) \sinh\left(\frac{1}{2}\lambda_1 L_v\right) + \sin\left(\frac{1}{2}\lambda_1 L_b\right) \sin\left(\frac{1}{2}\lambda_1 L_v\right)\right)\bigg). \end{aligned} \tag{48b}$$

Then from Eqs. (44) and (45) we have

$$z_{bs}\left(\frac{L_b}{2}\right) \cong Q_{b\text{mid}} + Q_{r\text{mid}}, \tag{49a}$$

$$z_{rs}\left(\frac{L_b}{2}\right) \cong -1.2119\left(\psi_{11} Q_{b\text{mid}} + \psi_{12} Q_{r\text{mid}}\right). \tag{49b}$$

According to different acting place of the moving load, the midpoint displacement of the rail and bridge can be expressed as the following three conditions:

$$(1)\ z_{bd}\left(\frac{L_b}{2}, t\right) \cong Q_{ub} + Q_{ur}, \quad z_{rd}\left(\frac{L_b}{2}, t\right) \cong -1.2119\left(\psi_{11} Q_{ub} + \psi_{12} Q_{ur}\right), \tag{50a,b}$$

$$(2)\ z_{bd}\left(\frac{L_b}{2}, t\right) \cong Q_{ab} + Q_{ar}, \quad z_{rd}\left(\frac{L_b}{2}, t\right) \cong -1.2119\left(\psi_{11} Q_{ab} + \psi_{12} Q_{ar}\right), \tag{51a,b}$$

$$(3)\ z_{bd}\left(\frac{L_b}{2}, t\right) \cong Q_{ob} + Q_{or}, \quad z_{rd}\left(\frac{L_b}{2}, t\right) \cong -1.2119\left(\psi_{11} Q_{ob} + \psi_{12} Q_{or}\right). \tag{52a,b}$$

The corresponding impact factors are known as

$$(1)\ I_b = \frac{Q_{ub} + Q_{ur}}{Q_{b\mathrm{mid}} + Q_{r\mathrm{mid}}} - 1, \quad I_r = \frac{\psi_{11} Q_{ub} + \psi_{12} Q_{ur}}{\psi_{11} Q_{b\mathrm{mid}} + \psi_{12} Q_{r\mathrm{mid}}} - 1, \tag{53a,b}$$

$$(2)\ I_b = \frac{Q_{ab} + Q_{ar}}{Q_{b\mathrm{mid}} + Q_{r\mathrm{mid}}} - 1, \quad I_r = \frac{\psi_{11} Q_{ab} + \psi_{12} Q_{ar}}{\psi_{11} Q_{b\mathrm{mid}} + \psi_{12} Q_{r\mathrm{mid}}} - 1, \tag{54a,b}$$

$$(3)\ I_b = \frac{Q_{ob} + Q_{or}}{Q_{b\mathrm{mid}} + Q_{r\mathrm{mid}}} - 1, \quad I_r = \frac{\psi_{11} Q_{ob} + \psi_{12} Q_{or}}{\psi_{11} Q_{b\mathrm{mid}} + \psi_{12} Q_{r\mathrm{mid}}} - 1. \tag{55a,b}$$

## 5. Numerical analysis

Previous sections have given the approximate solutions of the guideway. This section discusses the analyzing results. Three problems need to be studied: (1) The relationship between natural frequency and structural parameters; (2) midpoint displacement of the guideway induced by the moving vehicle; (3) impact factor of the midpoint displacement. Numerical calculation shows that the second natural frequency of the $n$th mode is larger than the first one (20 times), which means that the influence of the first one to the system is greater than that of the second one. Thus only the first one needs to be discussed. As is given in Fig. 2, the properties of the guideway investigated here are listed in Table 1 and we set $k_{sle} = 6.958 \times 10^6\,\mathrm{N/m^2}$. As can be seen from Table 2, the first three natural frequency calculated from the analytical solutions of (19) agree quit well with those by solving the free vibration problem of (14) using the first 10 sets of assumed displacement functions. In Table 2, $\Omega_{1,1}$ ($i = 1,2,3$) represents the first natural frequency of the $i$th mode.

Fig. 2(a) and (b) shows the first three modes of the rail and bridge. The first, second and third modes correspond to $\Omega_{1,1}$, $\Omega_{2,1}$ and $\Omega_{3,1}$. It is noted that Fig. 2(a) gives the zero mode of the rail corresponding to $\lambda_0 = 0$. It means that the rail lying on the elastic foundation with two ends free can move like rigid body [18].

An observation of (13) indicates that it is a set of coupled differential equations for all the symmetric modes; the closed-form solutions for the displacement response of the guideway are hard to derive. Therefore, a numerical evaluation based on Wilson-$\theta$ numerical integration method will be employed to solve the dynamic response of the generalized coordinates ($q_{r,n}$,$q_{b,n}$). To improve the accuracy of the dynamic response of the guideway subjected to moving load, the first 10 sets of assumed displacement modes are considered for the deflection curves of the guideway, namely letting $n = 10$. The solution obtained in this way will be used as the basis of comparison in the numerical studies.

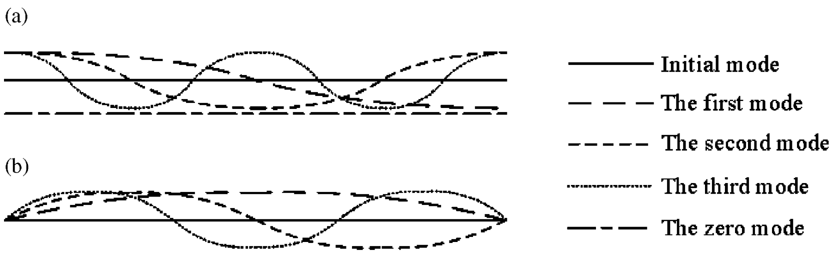


Fig. 2. Natural modes of the guideway: (a) rail mode; (b) bridge mode.

Table 1
Properties of the rail and bridge

| | $L_b$ (m) | $EI$ (N m$^2$) | $\rho$ (kg/m) | $C$ (N s/m$^2$) |
|---|---|---|---|---|
| Rail | 24 | $2.7993 \times 10^{10}$ | 103 | 0.001 |
| Bridge | 24 | $9 \times 10^9$ | 2697 | 0.008 |

Table 2
Natural frequencies of the guideway

| Frequency | $\Omega_{1,1}$ (rad/s) | $\Omega_{2,1}$ (rad/s) | $\Omega_{3,1}$ (rad/s) |
|---|---|---|---|
| Eq. (19) | 59.6387 | 139.115 | 286.2565 |
| Multiple sets of vibration modes | 59.6387 | 139.1149 | 286.2517 |

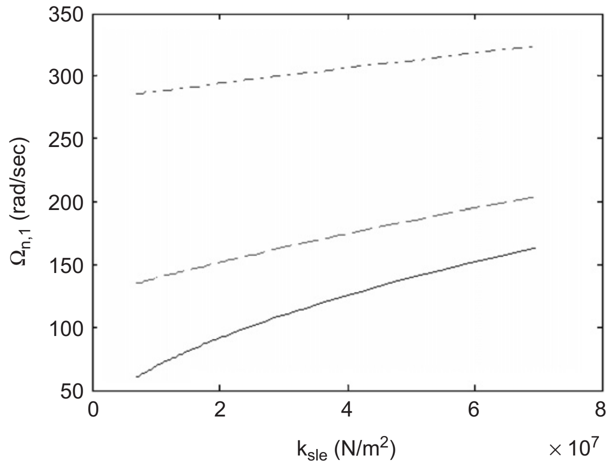


Fig. 3. Relationship between the first natural frequencies and sleeper stiffness (——) $\Omega_{1,1}$, (– – –) $\Omega_{2,1}$, (— · ) $\Omega_{3,1}$.

### 5.1. Effect of the structure parameter to natural frequency

Vehicle–guideway interaction may take place when the natural frequency of the controlled maglev system is close to the natural frequency of the guideway [19]. By investigating the influence of the structure parameter to the natural frequency of the guideway, we are able to grasp the mechanism of the vehicle–guideway interaction and the method to suppress the coupling resonance. When the free ends beam is supported by the elastic foundation, natural frequencies are influenced by the stiffness of the foundation [18]. Fig. 3 proves this result again. With different stiffness of the elastic foundation, the first natural frequencies of the guideway increases with the stiffness of the sleeper going large.

Beam stiffness influences the natural frequencies either, as is shown in Fig. 4. In Fig. 4(a), when $E_bI_b$ is small, the first three natural frequencies are close to each other. With the increase of $E_bI_b$, the increasing speed of $\Omega_{1,1}$ is the smallest while $\Omega_{3,1}$ increases the fastest which implies that the higher the mode is, the faster the natural frequency increases. The stiffness of rail $E_rI_r$ almost does not affect the natural frequency.

How does mass per unit length of the guideway affect the natural frequencies has not yet been clearly illustrated. In general, mass per unit length has straight connection with the bending stiffness of the beam. The larger mass per unit length is, the stiffer the beam will becomes. And engineering cost will go higher with the increase of mass per unit length. So this relation is much valuable for engineering procedure. Fig. 5 presents the numerical relationship between natural frequencies and mass per unit length. As observed in Fig. 5(a), natural frequencies decrease with the increase of mass per unit length of the bridge, and the higher the mode is, the faster the frequencies will decrease. The influence of mass per unit length of the rail to the natural frequencies can be omitted.

### 5.2. Midpoint displacement and impact response of the maglev guideway

To illustrate the vibration phenomenon of the guideway under action of the evenly distributed load, setting $v = 27.78\,\mathrm{m/s}(100\,\mathrm{km/h})$, $f_m = 22400\,N$, $L_v = 12\,m$. Wilson-$\theta$ numerical integral method is employed with

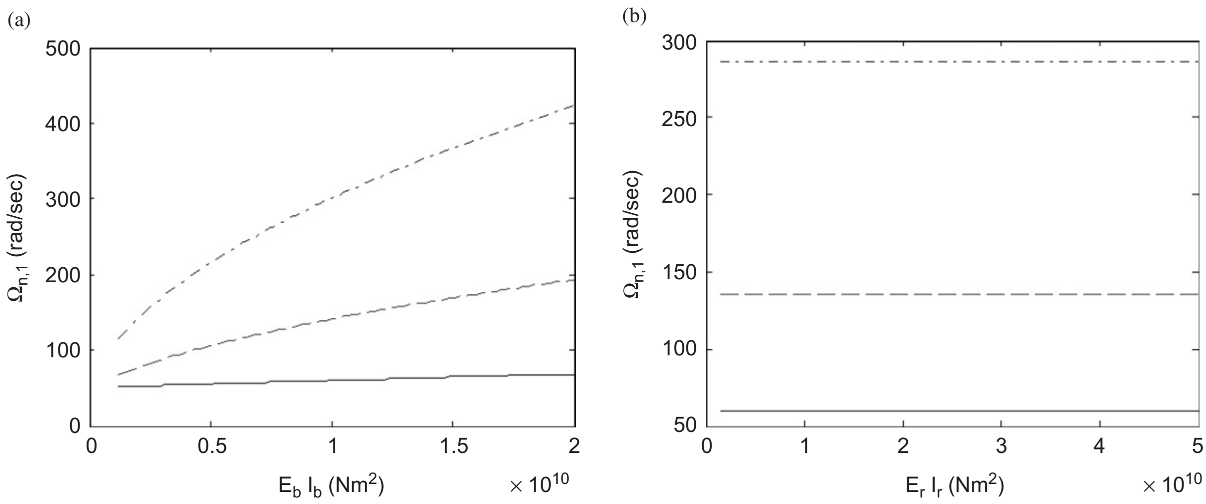


Fig. 4. Relationship between the first natural frequencies and stiffness of the guideway: (a) $E_bI_b$—$\Omega_{n,1}$ curves; (b) $E_rI_r$—$\Omega_{n,1}$ curves. (——) $\Omega_{1,1}$, (– – –) $\Omega_{2,1}$, (— · ) $\Omega_{3,1}$.

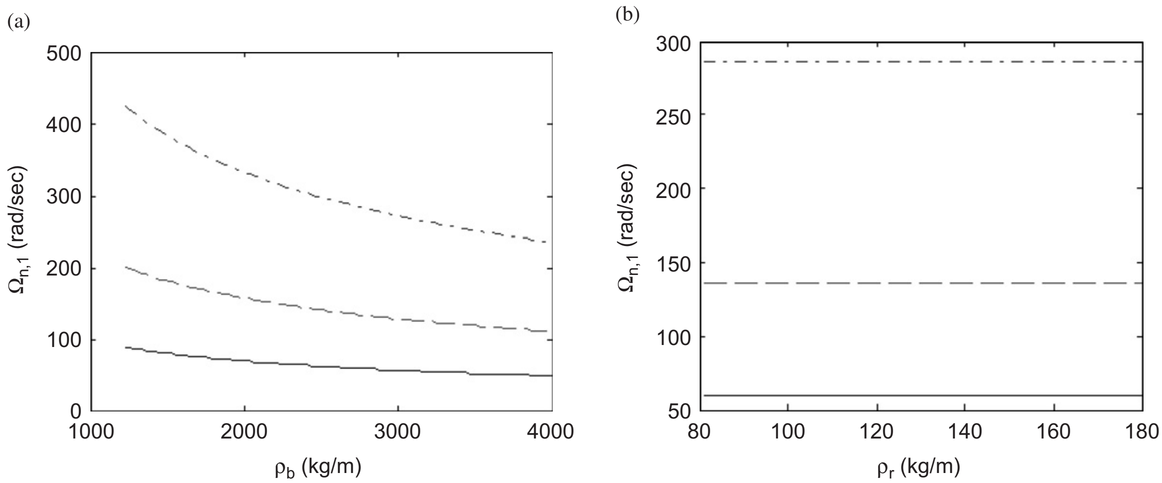


Fig. 5. Relationship between the first natural frequencies and mass per unit length of the guideway : (a) $\rho_b$—$\Omega_{n,1}$ curves; (b) $\rho_r$—$\Omega_{n,1}$ curves; (——) $\Omega_{1,1}$, (– – –) $\Omega_{2,1}$, (— · ) $\Omega_{3,1}$.

$\theta = 1.4$, the first 10 sets of assumed displacement modes are considered, and numerical result is compared with the analytical solutions (35), (39) and (42). Introducing the non-dimensional time factor $vt/L_b$, Figs. 6 and 7 show their comparison results. To the rail displacement, one mode analytical solution is in good agreement with the multimode numerical calculation. While the larger the displacement value is, the bigger the difference between analytical and numerical result will become. But the absolute value of the difference is small. When we study the deflection of the guideway, only considering the first mode will not differ much from considering multimodes. In addition, when $vt/L_b > 1.5$, evenly distributed load has run out of the bridge, the guideway will vibrate at low frequency. Because structure damping of the guideway is not zero, the free vibration will vanish anyway. Since sleeper can isolate the vibration, the vibration amplitude of the rail is much smaller than that of the bridge.

Displacement impact response of the Guideway subjecting the moving load can be reflected by only analyzing the first mode when the guideway is simply supported [15]. Eq. (51) gives the expression of the guideway displacement impact factor for the first mode. To illustrate the effect of the acting position $vt$

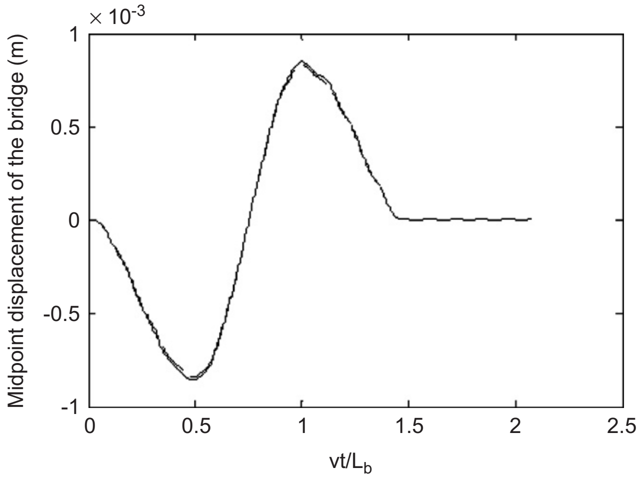


Fig. 6. Midpoint displacement of the bridge, (——) the first mode approximation, (— —) multiple mode approximation.

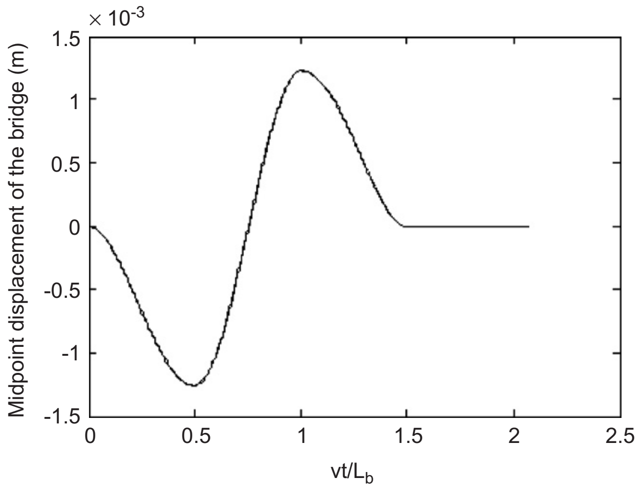


Fig. 7. Midpoint displacement of the rail, (——) the first mode approximation, (— —) multiple mode approximation.

of the moving load, different values have been assumed for $vt$, i.e., $vt/L_b = 0.1,0.3,0.5,0.7,0.9$. Figs. 8 and 9 show the impact factor of the dynamic response of the guideway to the static displacement of the midpoint. The maximal speed is set to be 1500 km/h, which has never been met by track vehicles and is big enough. With different acting position, impact factor differs much. From Fig. 8, we know that dynamic displacement of the guideway under the distributed moving load is always smaller than the maximum static displacement of the guideway midpoint. And in the midpoint of the span, the dynamic displacement is the biggest. Several extreme values of the displacement are obtained as can be seen from the curves. And with different acting place, the speeds to induce the extreme values are different either. In Fig. 8, when $vt/L_b = 0.1,0.3,0.5,0.7$, once the impact factor reaches its maximum value, it will decrease with the increase of the speed. Namely at some place of the bridge, the max dynamic displacement of the guideway will increase when the speed of the load decreases. This is in agreement with some experimental phenomena. Numerical simulation of (13) has testified this trend. Impact curves in Fig. 9 are meeker than those in Fig. 8, no apparent peaks exist in the plot when $S<0.3$. This implies that moving load will not impact the rail strongly because of the elastic foundation. Thus, only the impact response of the bridge needs to be carefully considered.

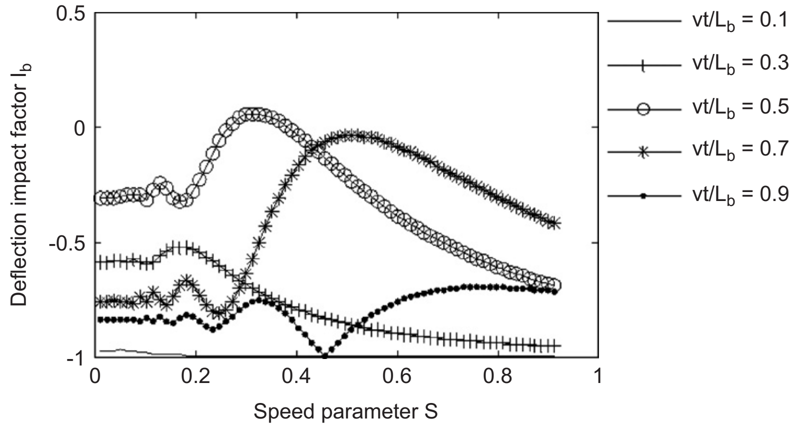


Fig. 8. $I_b$–$S$ plot of the bridge due to moving load.

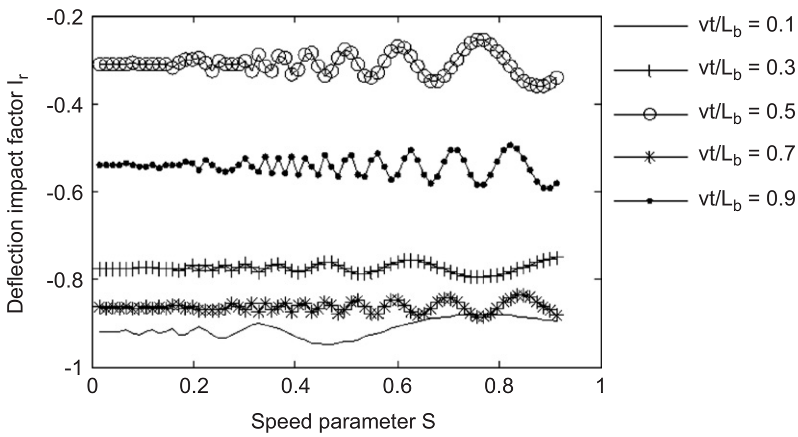


Fig. 9. $I_r$–$S$ plot of the tail due to moving load.

## 6. Future research and conclusions

Vehicle–guideway interaction of the maglev system is an important and complicated problem. It is influenced by the levitation system, guideway structure, vehicle structure, running speed, etc. So the investigation of it should be launched out in many aspects. This article only concerns the dynamic response of the guideway, the effects of the vehicle structure and controlling system are neglected. In the future work, elasticity of the concrete supports, variation of the sleepers' stiffness and the style of the guideway, the relation between maglev control system and the vibration of the guideway and the second suspension system, etc. are necessary to study. A great amount of work will be carried out.

This paper studies the dynamic response of the maglev guideway subjecting the evenly distributed moving load by using the mode superposition method. The model of the guideway composed of the rail–elastic foundation–simply supported beam is built for the first time. It is pointed out that stiffness of the sleeper bridge and mass per unit length of the bridge greatly influence the value of natural frequency. If the natural frequency of the maglev system and the guideway is close enough, vehicle–guideway interaction is easy to appear. So properly select the structure parameter of the guideway is helpful to suppress the resonant phenomenon. Closed-form solutions of the guideway imply that vehicle–guideway interaction is not necessarily occurring with the maglev vehicle passing through the bridge with constant speed. Analytical result of the impact factor shows that when running speed of the load closes to certain values, the displacement of the rail and bridge will reach their local extreme value. These speed need to be avoided. Especially, at some position of the guideway, the dynamic displacement of the rail and bridge will decrease with the increase of the running speed and the dynamic displacements are always smaller than the maximal static midpoint displacement of the beam. Numerical simulation to the model with multimodes has testified these conclusions.

## Acknowledgments

The authors gratefully acknowledge the financial support for this work provided by National Nature and Science Foundation of China (NNSFC, No. 60404003) and Fok Ying Dong Education Foundation (FYDEF, No. 94028). Great thanks are given to J.D. Yau for his enthusiastic instruction.

## Appendix

$p_{ub0}$–$p_{ub7}$ in Eq. (34a) are shown below:

$$\begin{aligned}
&p_{ub0} = \left(m_b\omega_1^2 + k_b\right)^2 - c_b^2\omega_1^2, \quad p_{ub1} = c_b\omega_1 + m_b V_1\omega_1^2 + V_1 k_b,\\
&p_{ub2} = c_b^2\omega_1 + c_b V_1 k_b - m_b^2\omega_1^3 - m_b\omega_1 k_b, \quad p_{ub3} = -m_b\omega_1^3 - k_b\omega_1 - V_1 c_b\omega_1^2,\\
&p_{ub4} = c_b^2\omega_1^2 + m_b^2\omega_1^4 - 2k_b m_b\omega_1^2 + k_b^2, \quad p_{ub5} = m_b V_1\omega_1^2 - V_1 k_b - c_b\omega_1,\\
&p_{ub6} = m_b\omega_1 k_b - m_b^2\omega_1^3 - c_b^2\omega_1 - c_b V_1 k_b, \quad p_{ub7} = m_b\omega_1^3 - k_b\omega_1 + V_1 c_b\omega_1^2.
\end{aligned}$$

$p_{ur0}$–$p_{ur7}$ in Eq. (34b) are shown below:

$$\begin{aligned}
&p_{ur0} = \left(m_r\omega_1^2 + k_r\right)^2 - c_r^2\omega_1^2, \quad p_{ur1} = c_r\omega_1 + m_r V_1\omega_1^2 + V_1 k_r,\\
&p_{ur2} = c_r^2\omega_1 + c_r V_1 k_r - m_r^2\omega_1^3 - m_r\omega_1 k_r, \quad p_{ur3} = -m_r\omega_1^3 - k_r\omega_1 - V_1 c_r\omega_1^2,\\
&p_{ur4} = c_r^2\omega_1^2 + m_r^2\omega_1^4 - 2k_r m_r\omega_1^2 + k_r^2, \quad p_{ur5} = m_r V_1\omega_1^2 - V_1 k_r - c_r\omega_1,\\
&p_{ur6} = m_r\omega_1 k_r - m_r^2\omega_1^3 - c_r^2\omega_1 - c_r V_1 k_r, \quad p_{ur7} = m_r\omega_1^3 - k_r\omega_1 + V_1 c_r\omega_1^2.
\end{aligned}$$

$a_1$–$a_4$ in Eq. (36) are given as follows:

$$\begin{aligned}
&a_1 = \frac{f_m}{\lambda_1}(1 - \cosh(\lambda_1 L_v) - V_1\sinh(\lambda_1 L_v)), \quad a_2 = \frac{f_m}{\lambda_1}(1 - \cos(\lambda_1 L_v) - V_1\sin(\lambda_1 L_v)),\\
&a_3 = \frac{f_m}{\lambda_1}(-V_1 + \sinh(\lambda_1 L_v) + V_1\cosh(\lambda_1 L_v)), \quad a_4 = \frac{f_m}{\lambda_1}(V_1 + \sin(\lambda_1 L_v) - V_1\cos(\lambda_1 L_v)).
\end{aligned}$$

$p_{ab0}$–$p_{ab7}$ in Eq. (38a) are shown as

$$\begin{aligned}
&p_{ab0} = \left(m_b\omega_1^2 + k_b\right)^2 - c_b^2\omega_1^2, \quad p_{ab1} = a_1 c_b\omega_1 - m_b a_3\omega_1^2 - a_3 k_b,\\
&p_{ab2} = c_b^2\omega_1 a_1 - c_b a_3 k_b - m_b^2\omega_1^3 a_1 - m_b\omega_1 k_b a_1, \quad p_{ab3} = -a_3 c_b\omega_1^2 + a_1 m_b\omega_1^3 + \omega_1 a_1 k_b,\\
&p_{ab4} = c_b^2\omega_1^2 + m_b^2\omega_1^4 - 2k_b m_b\omega_1^2 + k_b^2, \quad p_{ab5} = m_b a_4\omega_1^2 - a_4 k_b - a_2 c_b\omega_1,\\
&p_{ab6} = m_b^2\omega_1^3 a_2 - m_b\omega_1 k_b a_2 + c_b^2\omega_1 a_2 - c_b k_b a_4, \quad p_{ab7} = -m_b\omega_1^3 a_2 + \omega_1 k_b a_2 + a_4 c_b\omega_1^2.
\end{aligned}$$

$p_{ar0}$–$p_{ar7}$ in Eq. (38b) are shown as

$$\begin{aligned}
&p_{ar0} = \left(m_r\omega_1^2 + k_r\right)^2 - c_r^2\omega_1^2, \quad p_{ar1} = a_1 c_r\omega_1 - m_r a_3\omega_1^2 - a_3 k_r,\\
&p_{ar2} = c_r^2\omega_1 a_1 - c_r a_3 k_r - m_r^2\omega_1^3 a_1 - m_r\omega_1 k_r a_1, \quad p_{ar3} = -a_3 c_r\omega_1^2 + a_1 m_r\omega_1^3 + \omega_1 a_1 k_r,\\
&p_{ar4} = c_r^2\omega_1^2 + m_r^2\omega_1^4 - 2k_r m_r\omega_1^2 + k_r^2, \quad p_{ar5} = m_r a_4\omega_1^2 - a_4 k_r - a_2 c_r\omega_1,\\
&p_{ar6} = m_r^2\omega_1^3 a_2 - m_r\omega_1 k_r a_2 + c_r^2\omega_1 a_2 - c_r k_r a_4, \quad p_{ar7} = -m_r\omega_1^3 a_2 + \omega_1 k_r a_2 + a_4 c_r\omega_1^2.
\end{aligned}$$

$O_0$–$O_4$ in Eq. (40) are shown below:

$$o_0 = \frac{f_m}{\lambda_1}(\sinh(\lambda_1 L_b) + \sin(\lambda_1 L_b) - V_1\cosh(\lambda_1 L_b) + V_1\cos(\lambda_1 L_b)) = 0,$$
$$o_1 = \frac{f_m}{\lambda_1}(-\cosh(L_v\lambda_1) - V_1\sinh(L_v\lambda_1)),$$
$$o_2 = \frac{f_m}{\lambda_1}(-\cos(L_v\lambda_1) - V_1\sin(L_v\lambda_1)),$$
$$o_3 = \frac{f_m}{\lambda_1}(\sinh(L_v\lambda_1) + V_1\cosh(L_v\lambda_1)), \quad o_4 = \frac{f_m}{\lambda_1}(\sin(L_v\lambda_1) - V_1\cos(L_v\lambda_1)).$$

$p_{ob0}$–$p_{ob7}$ in Eq. (42a) are shown as

$$p_{ob0} = \left(m_b\omega_1^2 + k_b\right)^2 - c_b^2\omega_1^2, \quad p_{ob1} = o_1c_b\omega_1 - m_bo_3\omega_1^2 - o_3k_b,$$
$$p_{ob2} = c_b^2\omega_1o_1 - c_bo_3k_b - m_b^2\omega_1^3o_1 - m_b\omega_1k_bo_1, \quad p_{ob3} = -o_3c_b\omega_1^2 + o_1m_b\omega_1^3 + \omega_1o_1k_b,$$
$$p_{ob4} = c_b^2\omega_1^2 + m_b^2\omega_1^4 - 2k_bm_b\omega_1^2 + k_b^2, \quad p_{ob5} = m_bo_4\omega_1^2 - o_4k_b - o_2c_b\omega_1,$$
$$p_{ob6} = m_b^2\omega_1^3o_2 - m_b\omega_1k_bo_2 + c_b^2\omega_1o_2 - c_bk_bo_4, \quad p_{ob7} = -m_b\omega_1^3o_2 + \omega_1k_bo_2 + o_4c_b\omega_1^2.$$

$p_{or0}$–$p_{or7}$ in Eq. (42b) are shown as

$$p_{or0} = \left(m_r\omega_1^2 + k_r\right)^2 - c_r^2\omega_1^2, \quad p_{or1} = o_1c_r\omega_1 - m_ro_3\omega_1^2 - o_3k_r,$$
$$p_{or2} = c_r^2\omega_1o_1 - c_ro_3k_r - m_r^2\omega_1^3o_1 - m_r\omega_1k_ro_1, \quad p_{or3} = -o_3c_r\omega_1^2 + o_1m_r\omega_1^3 + \omega_1o_1k_r,$$
$$p_{or4} = c_r^2\omega_1^2 + m_r^2\omega_1^4 - 2k_rm_r\omega_1^2 + k_r^2, \quad p_{or5} = m_ro_4\omega_1^2 - o_4k_r - o_2c_r\omega_1,$$
$$p_{or6} = m_r^2\omega_1^3o_2 - m_r\omega_1k_ro_2 + c_r^2\omega_1o_2 - c_rk_ro_4, \quad p_{or7} = -m_r\omega_1^3o_2 + \omega_1k_ro_2 + o_4c_r\omega_1^2.$$

## References


[1] Y. Cai, S.S. Chen, Dynamic characteristics of magnetically levitated vehicle systems, *Applied Mechanics Reviews* 50 (11) (1997) 647–670.

[2] Y. Cai, S.S. Chen, D.M. Rote, Vehicle/guideway interaction for high speed vehicles on a flexible guideway, *Journal of Sound and Vibration* 175 (5) (1994) 625–646.

[3] Y. Cai, S.S. Chen, D.M. Rote, Vehicle/guideway dynamic interaction in maglev systems, *Journal of Dynamic Systems Measurement and Control—Transactions of the ASME* 18 (5) (1996) 526–530.

[4] C.F. Zhao, W.M. Zhai, Dynamics of maglev vehicle/guideway system(II)—modeling and simulation, *Chinese Journal of Mechanical Engineering* 41 (8) (2005) 163–175.

[5] X.J. Zheng, J.J. Wu, Y.-H. Zhou, Numerical analyses on dynamic control of five-degree-of freedom maglev vehicle moving on flexible guideways, *Journal of Sound and Vibration* 235 (2000) 43–61.

[6] X.J. Zheng, J.J. Wu, Y.-H. Zhou, Effect of spring non-linearity on dynamic stability of a controlled maglev vehicle and guideway system, *Journal of Sound and Vibration* 279 (2005) 201–215.

[7] Y.B. Yang, C.L. Lin, J.D. Yau, D.W. Chang, Mechanism of resonance and cancellation for train-induced vibrations on bridges with elastic bearings, *Journal of Sound and Vibration* 269 (2004) 345–360.

[8] Y.B. Yang, C.W. Lin, Vehicle–bridge interaction dynamics and potential applications, *Journal of Sound and Vibration* 284 (2005) 205–226.

[9] J.D. Yau, Y.B. Yang, Vertical accelerations of simple beams due to successive loads traveling at resonant speeds, *Journal of Sound and Vibration* 289 (2006) 210–228.

[10] J.D. Yau, Vibration of parabolic tied-arch beams due to moving loads, *International Journal of Structural Stability and Dynamics* 6 (2) (2006) 193–214.

[11] L. Baeza, A. Roda, J.C.O. Nielsen, Railway vehicle/track interaction analysis using a modal substructuring approach, *Journal of Sound and Vibration* 293 (2006) 112–124.

[12] B. Biondi, G. Muscolino, A. Sofi, A substructure approach for the dynamic analysis of train–track–bridge system, *Computers & Structures* 83 (2005) 2271–2281.

[13] M. Shamalta, A.V. Metrikine, Analytical study of the dynamic response of an embedded railway track to a moving load, *Archive of Applied Mechanics* 73 (2003) 131–146.

[14] S. Kaewunruen, A.M. Remennikov, Sensitivity analysis of free vibration characteristics of an in situ railway concrete sleeper to variations of rail pad parameters, *Journal of Sound and Vibration* 298 (2006) 453–461.
[15] Y.B. Yang, J.D. Yau, Y.S. Wu, *Vehicle–Bridge Interaction Dynamics with Applications to High-Speed Railways*, World Scientific, Singapore, 2004.
[16] H. Xia, N. Zhang, *Dynamic Interaction of Vehicles and Structures*, Science Press, Moscow, 2005.
[17] R.W. Clough, J. Penzien, *Dynamics of Structures*, McGraw-Hill, New York, 1993.
[18] S. Timoshenko, D.H. Young, W. Weaver, *Vibration Problems in Engineering*, Vol. 4e, Wiley, New York, 1974.
[19] P.K. Sinha, *Electromagnetic Suspension Dynamics & Control*, Peter Peregrinus Ltd., London, 1987.